Bioorganic & Medicinal Chemistry Letters 22 (2012) 5876–5884

Contents lists available at SciVerse ScienceDirect

Bioorganic & Medicinal Chemistry Letters

journal homepage: www.elsevier.com/locate/bmcl

Novel triazines as potent and selective phosphodiesterase 10A inhibitors ☆

Michael S. Malamas [a,†,*], Hans Stange [b], Rudolf Schindler [b], Hans-Joachim Lankau [b], Christian Grunwald [b], Barbara Langen [b], Ute Egerland [b], Thorsten Hage [b], Yike Ni [a], James Erdei [a], Kristi Yi Fan [a,§], Kevin Parris [a,††], Karen L. Marquis [a], Steve Grauer [a], Julie Brennan [a], Rachel Navarra [a], Radka Graf [a], Boyd L. Harrison [a], Albert Robichaud [a,‡], Thomas Kronbach [b], Menelas N. Pangalos [a,¶], Nicholas J. Brandon [a,‖], Norbert Hoefgen [b,†]

[a] Pfizer Neuroscience Princeton, 865 Ridge Road, Monmouth Junction, NJ 08852, USA
[b] Biocrea, Meissner Strasse 191, 01445 Radebeul, Germany

ARTICLE INFO

Article history:
Available online 31 July 2012

Keywords:
Schizophrenia
PDE10A inhibitors
Triazines
MK-801

ABSTRACT

The identification of highly potent and orally active triazines for the inhibition of PDE10A is reported. The new analogs exhibit low-nanomolar potency for PDE10A, demonstrate high selectivity against all other members of the PDE family, and show desired drug-like properties. Employing structure-based drug design approaches, we investigated the selectivity of PDE10A inhibitors against other known PDE isoforms, by methodically exploring the various sub-regions of the PDE10A ligand binding pocket. A systematic assessment of the ADME and pharmacokinetic properties of the newly synthesized compounds has led to the design of drug-like candidates with good brain permeability and desirable drug kinetics ($t_{1/2}$, bioavailability, clearance). Compound **66** was highly potent for PDE10A (IC_{50} = 1.4 nM), demonstrated high selectivity (>200×) for the other PDEs, and was efficacious in animal models of psychoses; reversal of MK-801 induced hyperactivity (MED = 0.1 mg/kg) and conditioned avoidance responding (CAR; ID_{50} = 0.2 mg/kg).

Cyclic nucleotide phosphodiesterases (PDEs) are key regulators of cellular signal transduction by hydrolyzing the 3′, 5′-monophosphate bond of the intracellular second messengers adenosine 3′, 5′-monophosphate (cAMP[a]) and cyclic guanosine 3′, 5′-monophosphate (cGMP). There are 11 distinct phosphodiesterases, designated as PDE1 through PDE11.[1] PDEs are classified by their substrate specificity. Some selectively hydrolyze cAMP or cGMP, while others hydrolyze both substrates.[2,3] The PDEs are localized to specific sub-cellular sites, which allows for fine spatial and temporal control of the levels of the cyclic nucleotides.[4,5] This feature is thought to be an important contributing factor that allows the enzyme to influence selective intracellular signaling pathways in response to different stimuli, in spite of the ubiquitous intracellular distribution of the cyclic nucleotides. PDE10A is a dual substrate PDE.[6–9] PDE10A hydrolyzing both cAMP and cGMP, with a higher affinity for cAMP (K_m = 0.05 μM) than for cGMP (K_m = 3 μM).[10] PDE10A is primarily a membrane bound enzyme containing a catalytic domain in the C-terminal portion of the protein. Key residues of the catalytic core form a well-defined hydrophobic clamp region that positions the planar rings of the nucleotide for interaction with an absolutely conserved glutamine residue (Gln716 in PDE10A). Free rotation of this glutamine in PDE10A, and other dual substrate enzymes, is believed to allow the binding of either cAMP or cGMP in the substrate pocket.[11] PDE10A mRNA is highly expressed only in brain and testes.[7,8] In the brain, both PDE10A mRNA and protein are specifically enriched in the medium spiny neurons (MSNs) of the striatum.[12] Intriguingly, PDE10A expression looks to be fairly well conserved across species (mice, rats, dog, macaque and humans), which could be important for the translation of any rodent models into human efficacy.[13] PDE10A has been suggested to play a key role in regulating MSN activity and in turn striatal output as this region integrates dopaminergic and glutama-

Abbreviations: PDE10A, phosphodiesterase 10A; cAMP, cyclic adenosine monophosphate; cGMP, cyclic guanine monophosphate; MSN, medium spiny neuron; MK-801, dizocilpine maleate; MED, minimal effective dose; PDE, cyclic nucleotide phosphodiesterase; LMA, locomotor activity; CAR, conditioned avoidance response.

☆ Atomic coordinates of the PDE10 crystal structure with compounds 4 (4FCB) and 48 (4FCD) have been deposited in the Protein Data Bank, Research Collaboratory for Structural Bioinformatics, Rutgers University, New Brunswick, New Jersey.

* Corresponding author.
E-mail address: malamas.michael@gmail.com (M.S. Malamas).
† These authors contributed equally to the work.
‡ Present address: Sage Therapeutics, Cambridge, MA.
§ Present address: Vitae Pharmaceuticals, Fort Washington, PA.
¶ Present address: AstraZeneca, Alderley Park, SK10 4TG, UK.
‖ Present address: AstraZeneca Neuroscience iMED, Boston, MA.
†† Present address: Pfizer Neuroscience, Eastern Point Road, Groton CT.

0960-894X/$ - see front matter © 2012 Elsevier Ltd. All rights reserved.
http://dx.doi.org/10.1016/j.bmcl.2012.07.076

tergic inputs from midbrain and cortical regions, respectively, to action motoric and cognitive function. Dysfunction in cortical–striatal neurotransmission has been implicated in the pathophysiology of schizophrenia and Huntingdon's disease, thus PDE10A inhibition has been suggested as a therapeutic strategy for this disease.[14–17]

In recent disclosures,[18,19] we have described the design of pyridyl- and phenyl-[2,3-e]pyrazines (**1**, **2**; Fig. 1) as potent inhibitors ($IC_{50} \sim$ 50-500 pM) of PDE10A, with high selectivity (>500×) for the other known PDE isoforms, with the exception of PDE2, which are less selective (~50–200×). The reported research, which was based on structure-based drug design approaches, has provided a better understanding of the requirements needed to enhance the ligand's potency and selectivity. Furthermore, other reports[20] on PDE10A inhibitors (exemplified by compound **3**; Fig. 1), which are highly selective (~1000×) for all PDE isoforms, have revealed that the enhanced PDE2 selectivity of this class of compounds was attributed to the access of the ligand to a lipophilic pocket near the entrance of the hydrophobic cleft that defines the common PDE substrate binding site. A comparison of the known PDE crystal structures and profiling the inhibitor binding site suggested that this class of PDE10A ligands occupy this lipophilic pocket in an orientation that it is unique to PDE10A. The quinoline group of PDE10A inhibitor **3**, confirmed by X-ray crystallography studies,[20] extends deep into this lipophilic pocket and makes a hydrogen bond contact between the quinoline nitrogen and Tyr693 anchoring the inhibitor within the pocket. Only PDE10A has a small glycine residue at the entrance of this lipophilic pocket next to conserved Gln716, while all other PDEs have larger residues at the same position blocking the entrance of the ligand to this lipophilic 'selectivity' pocket. We have used this finding to further increase the selectivity of our PDE10A inhibitors (1, 2) versus PDE2. Using molecular modeling docking calculations, we were able to identify the attachment point (position 7) of the pyrazine scaffold (**4**; Fig. 1) to append a similar quinoline group to that found in **3**, and generate PDE10A potent inhibitor **4** (IC_{50} = 2.9 nM) with marked enhancement in PDE2 selectivity (>300×). To further support our molecular modeling calculations, compound **4** was then crystallized with PDE10A, and as shown in Figures 2a–b (PDB ID code 4FCB). In agreement with the molecular calculation studies the quinoline group extends deep toward the PDE10A 'selectivity' pocket and makes a direct contact between the quinoline nitrogen and Tyr683 (the difference in position numbering Tyr683 (in-house for **4**) versus Tyr693 (reported for **3**) is due to the different sequence numbering of the two resolved X-ray crystal structures). Furthermore, the fused ring system of the ligand is sandwiched between residues Phe719 and Phe686, making π-stacking interactions with Phe719 and hydrophobic contacts with Phe686. Also, the ligand extends toward the invariant Gln716 residue and makes a direct hydrogen bond contact between the pyrazine nitrogen and Gln716. The ligand is further stabilized within the binding pocket with additional water-mediated hydrogen bond interactions between the imidazole nitrogen and the residues Tyr514 and Asp664 (not shown). Several quinoline analogs were prepared and profiled (data not shown); however, despite the improved selectivity of the compounds against PDE2, the added molecular weight has negatively impeded on the ADME properties rendering these compounds not suitable as CNS drug candidates.

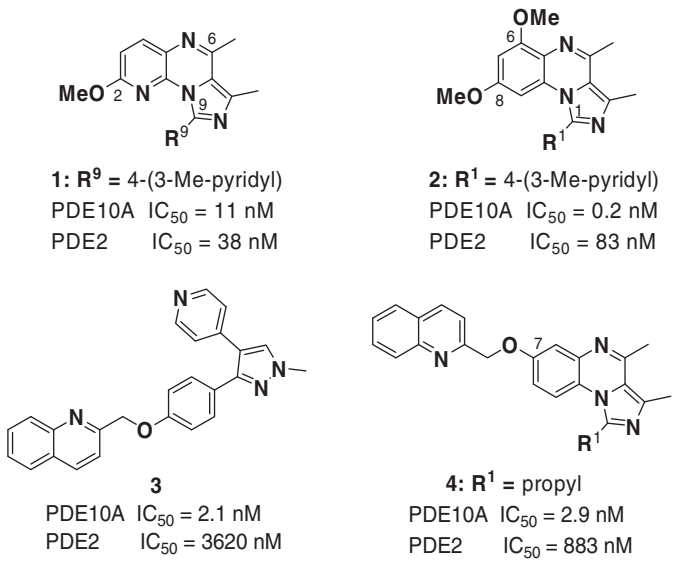

Figure 1. PDE10A inhibitors.

Next, we turned our attention to other approaches to increase selectivity against PDE2. Examination of the superimposed X-ray crystals of PDE2 (PDE2A PDB code 1Z1l) catalytic domain and PDE10A:**1** ($\mathbf{R_9}$ = propyl, PDB code 3LXG) (Fig. 3) revealed that the majority of the residues are identical in the active sites, except two residues around position 6 (Val668Gln and Ser667Asp). Furthermore, there is a large side chain movement for Ile682Ile close to position 9. Previous SAR studies[18,19] have suggested that various substitutions (i.e., OMe, CHF_2, CN, NH_2, and $NHSO_2Me$) at position 6 have only marginally affected the selectivity for PDE2. Also, it is noteworthy mentioning that smaller groups at position 6 showed tendency to be more selective against PDE2. At this point, we considered that a methodic SAR exploration of the various sub-regions of the PDE10A binding pocket could offer the opportunity to optimize the selectivity of our PDE10A inhibitors regarding PDE2 affinity.

In this Letter, we investigate the structural requirements critical for selectivity and disclose new triazine-based PDE10A inhibitors with an improved selectivity profile against PDE2. These new triazine inhibitors were developed in parallel with the pyridyl- and phenyl-[2,3-e]pyrazines inhibitors (1, 2), linking together key structure-activity relationship (SAR) findings and crystallographic driven structural features.

The compounds needed to delineate the SAR for this study were prepared according to synthetic Schemes 1–4. The described pyridyl-triazines (Table 1) were prepared according to Schemes 1 and 2. In Scheme 1 and 2-chloro-pyridine **5** was treated with 2-bromo-4-methyl imidazole in the presence of potassium hydroxide to afford the coupled product **6**. Reduction of the nitro group of **6** with stannous chloride produced aniline **7**. Cyclization of **7** to pyridyl-triazine **8** was accomplished with sodium nitrite and acetic acid. Intermediate **8** served as a building block for the preparation of synthetic libraries. Palladium-catalyzed cross coupling reaction of **8** with any number of aryl and heteroaryl boronic acids (Suzuki coupling[21]) in the presence of Pd(0) or Pd(II) catalyst under a variety of well known conditions produced the desired products **9** (entries 30–42; Table 1). The 4-methoxy analogs (entries 43–45; Table 1) were prepared according to Scheme 2. This synthetic protocol is closely related to that of Scheme 1; however, due to the decreased reactivity of **10** toward nucleophilic displacement, 4-methyl imidazole was used to couple with **10**. After separation of the 4:1 regioisomeric mixture, the major nitro intermediate **11** was reduced with iron to the aniline **12**. Cyclization of aniline **12** to pyrido-triazine **13** was accomplished with sodium nitrite and acetic acid. Bromination of **13** with N-bromosuccinimide produced bromo-imidazole **14**, which was further functionalized to the 4-methoxy analogs 43-45 (Table 1) using the Suzuki protocol as before. The synthetic approaches depicted in Scheme 3 and 4 were utilized for the preparation of the highly functionalized phenyl-triazine derivatives contained in Table 2. In Scheme 3, trifluoro-benzene **15** was treated with morpholine and potassium carbonate to

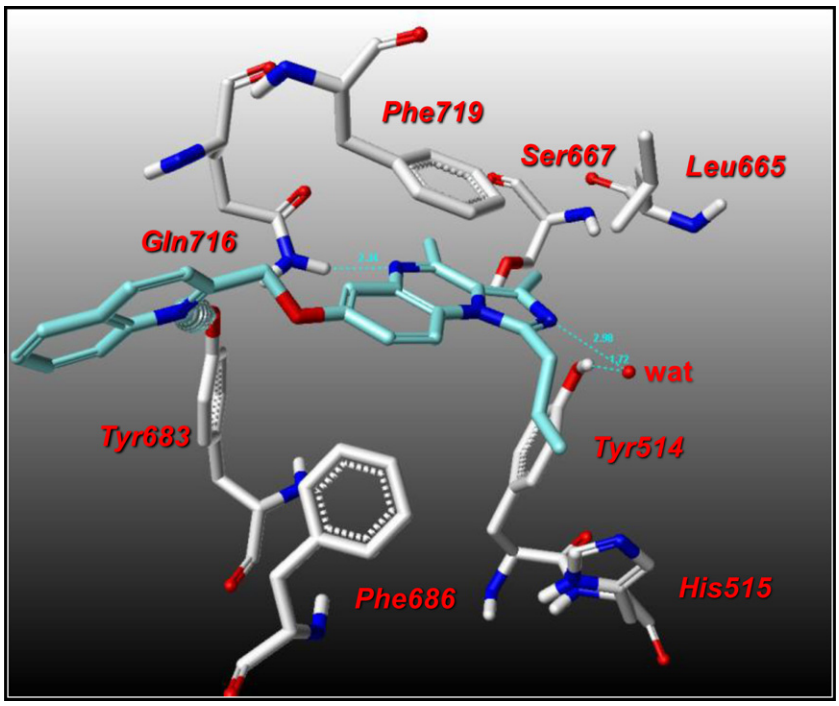

Figure 2a. Crystal structure (2.1 Å resolution; PDB ID code 4FCB) of PDE10A complexed with **4** highlighting the key hydrogen bond interactions between ligand and protein at the invariant Gln716 with the pyrazine nitrogen and the water-mediated contacts with Tyr514. The fused ring system of the ligand is sandwiched between residues Phe719, and Phe686, making p-stacking interactions with Phe719, pi-edge stacking with Phe686. The quinoline nitrogen makes a hydrogen bond interaction with Tyr663.

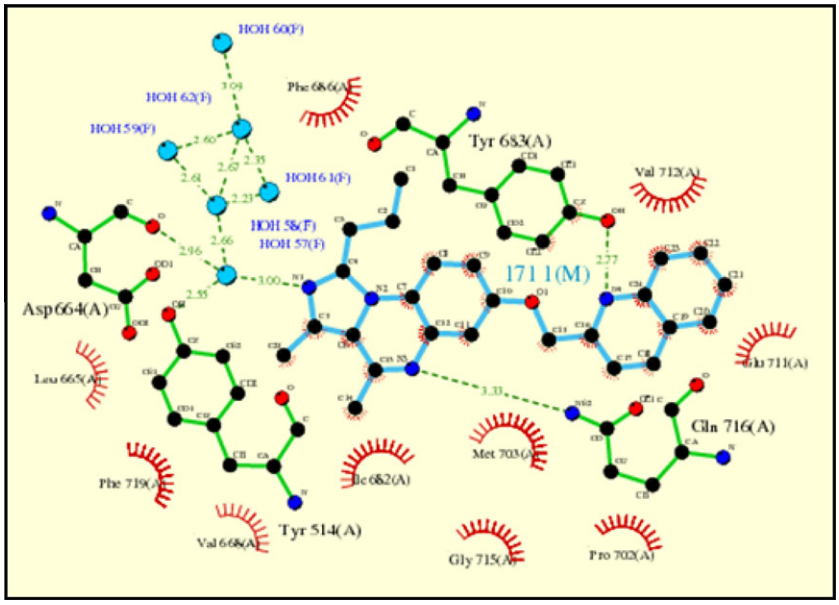

Figure 2b. Ligplot representation (2.1 Å resolution; PDB ID code 4FCB) of PDE10A complexed with **4** highlighting the hydrophobic and hydrogen bond interactions between the ligand and the amino acid residues involved in the PDE10A binding pocket.

produce **16**. Furthermore, aniline **17** was oxidized with sodium perborate to afford nitro benzene **18**. Intermediates **15**, **16** and**18** were coupled with 2-bromo-4-methyl imidazole, as described in Scheme 1, to furnish products **19**. Treatment of **19** with methanol and potassium hydroxide afforded the methoxy analogs **20**. Palladium-catalyzed cross coupling reaction of **20** with any number of aryl and heteroaryl boronic acids gave **21**. Reduction of the nitro intermediates **21** with ammonium formate and palladium on carbon afforded anilines **22**, which were further cyclized to phenyl-triazines **23** as before. The fluoro-methoxy analogs (entries 57–65, 70, 71 Table 2) were prepared according to Scheme 4. Phenol **24** was nitrated with fuming nitric acid to produce a mixture (1.5:1) of regioisomers **25** and **26**, which were separated and used as building blocks to generate the desired products **29** as described above in Schemes 1 and 2. The difluoromethoxy analog (entry **69**; Table 2) was prepared from nitro-phenol **24** upon alkylation with sodium chlorodifluoro acetate (forming difluoromethoxy group), and then applying the same synthetic protocols as described above in Schemes 1 and 2. Detailed experimental protocols of the compounds described in this Letter have been reported.[22]

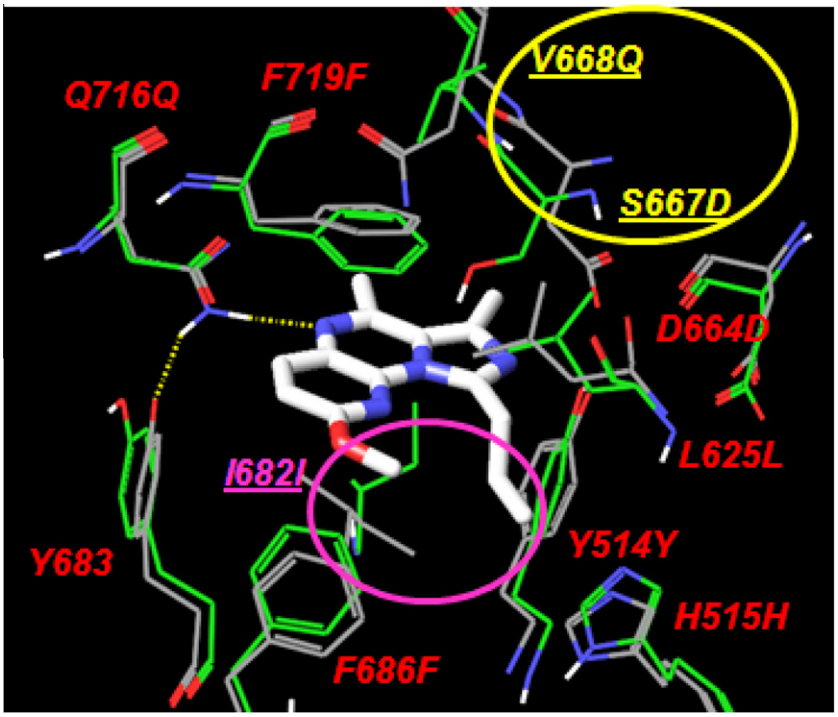

Figure 3. Superimposed X-ray crystals of PDE2A (grey; PDB ID code 1Z1 l) catalytic domain and PDE10A:**1** (*R* = propyl) co-crystal (green; PDB ID code 3LXG) reveal that the majority of the residues are identical in the active site, except two residues (yellow circle) Val668Gln and Ser667Asp. There is a large side chain movement for Ile682Ile (magenta circle).

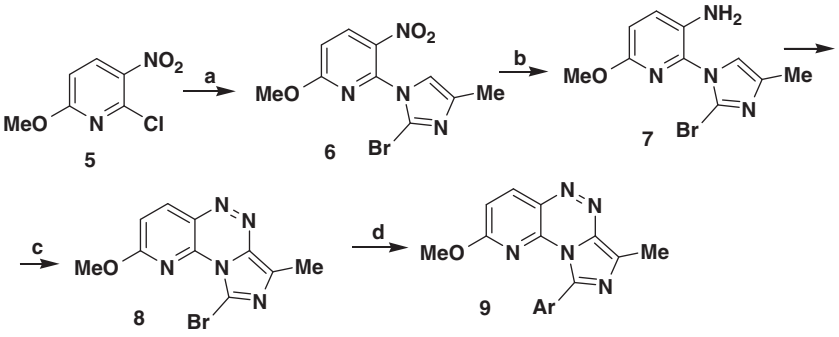

Scheme 1. Reagents: (a) 2-Br-4-Me-imidazole, KOH, DMF; (b) $SnCl_2$, EtOH; (c) $NaNO_2$, AcOH; (d) Ar-B$(OH)_2$, Pd$(PPh_3)_4$.

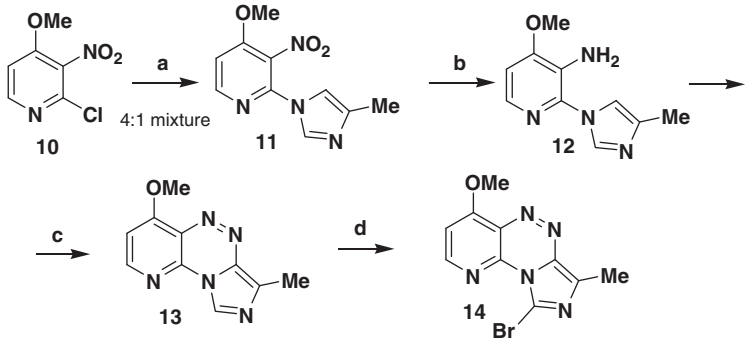

Scheme 2. Reagents: (a) 4-Me-imidazole, KOH, DMF; (b) Fe/AcOH, EtOH; (c) $NaNO_2$, AcOH; (d) NBS, AcCN.

Inhibitory potencies of our compounds were tested using in vitro inhibition of human recombinant PDE10A catalyzed cAMP hydrolysis.[19] We have routinely evaluated all compounds for selectivity against the PDE isoforms PDE2-PDE6, which have the potential for off-target liability. For matter of brevity, we are presenting our SAR evolution only in respect to PDE10A and those PDEs. How-

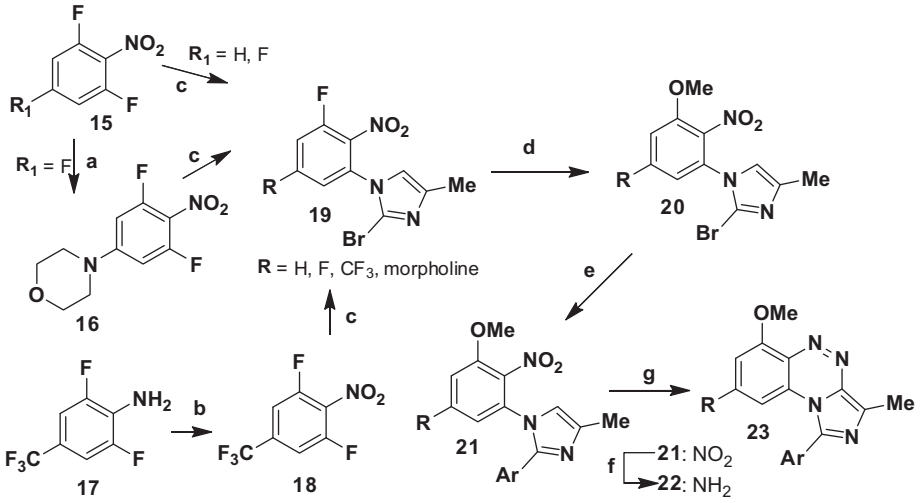

Scheme 3. Reagents: (a) morpholine, K_2CO_3, DMF; (b) $NaBO_3$, H_2O, AcOH; (c) 2-Br, 4-Me-imidazole, K_2CO_3, DMF; (d) KOH, MeOH; (e) Ar-$B(OH)_2$, $Pd(PPh_3)_4$; (f) HCO_2NH_4, Pd-C, MeOH; (g) $NaNO_2$, AcOH.

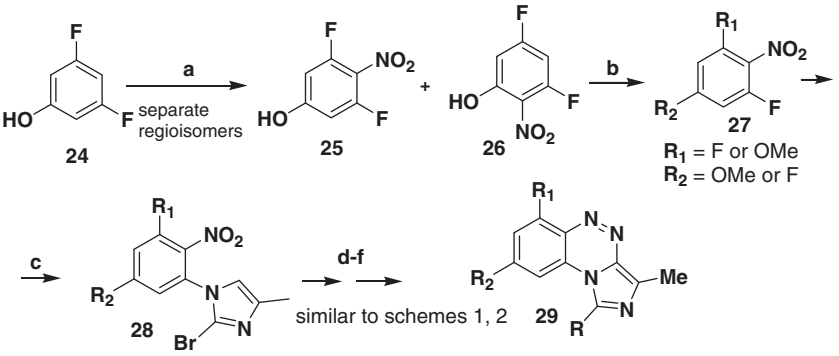

Scheme 4. Reagents: (a) HNO_3; (b) MeI, K_2CO_3; (c) 2-Br, 4-Me-imidazole, K_2CO_3, DMF; (d) Ar-$B(OH)_2$, $Pd(PPh_3)_4$; (e) Fe, AcOH; (f) $NaNO_2$, AcOH.

ever, if unexpected findings are emerging during the screening against the other PDEs (**1**, **7**–**9**, **11**), we are presenting these data appropriately. The results are compiled in Tables 1 and 2. The initial lead **1** ($\mathbf{R_9}$ = propyl, Fig. 1) was optimized[19] by using structure-based drug design techniques, primarily exploring the C9 and C6 positions of the pyridyl- (**1**) and phenyl- (**2**) pyrazines, respectively. The reported SAR exploration has resulted in >100-fold increase of the ligand's binding affinity for PDE10A, with enhanced selectivity >1000-fold for all other PDEs, with the exception of PDE2, where only a small subset of compounds showed selectivity ~100-fold. The SAR studies have indicated that substitutions at position 6 (phenyl-pyrazines; **2**) have contributed the most to the selectivity for PDE2. Other substitution positions that have also affected the selectivity versus PDE2 were positions 6 and 9 (pyridyl-pyrazines; **1**). As mentioned above, examination of the superimposed X-ray crystals of PDE2A (PDE2A PDB ID code 1Z1l) catalytic domain and PDE10A: **1** ($\mathbf{R_9}$ = propyl; PDB ID code 3LXG; Fig. 3) have revealed that the majority of the residues are identical in the active site, except two residues around position 6 (Val668Gln and Ser667Asp), with a large side chain movement for Ile682Ile close to position 9. In this Letter, we focus on analogs that lack a substitution at position 6 of the pyridyl-pyrazine (**1**) scaffold. It is notable, that the C6 des-methyl pyrazine analogs are rather weakly selective against PDE2 (data not shown). We have discovered that the triazine nucleus (Table 1) offered the opportunity to further investigate the PDE10A inhibitor potency and selectivity. In Table 1, we have aggregated selected analogs examining the effect of substitution at positions 2, 4 and 9 of the pyridyl-triazine scaffold (Table 1). Pyridyl analog **30** was weakly active, while the regioisomeric **31** was about 8–10× more active in both PDE10A and PDE2. The similarly substituted methoxy analog **32** was similar in potency to that of **31** (**32** vs **31**). Thiazole **33** was about 2× weaker in PDE2 to that of **31**. The methyl-substituted phenyl analogs **34** and **35** were similar in potency to that of **31**, while the halogen substituted-phenyl analogs **36**–**38** were about fivefold more potent in PDE10A. Interestingly, the dichloro analog **39**, while it did not show a change in PDE10A potency, it was sevenfold more potent in PDE2 with an IC_{50} value of 2 nM (**39** vs **34**). The fluoromethoxy phenyl analog **40** was potent in both PDE10A and PDE2. All phenyl analogs (**34**–**40**) were weakly active in the PDE3–PDE6 isoforms. An increase of the substitution size OEt versus OMe in analog **41** resulted in about 10-fold loss of potency for both PDE10A and PDE2 isoforms (**41** vs **40**). More pronounced was the potency loss (~200-fold) for the bulkier isopropyl analog **42** (**42** vs **40**). Moving the methoxy group from position 2 to position 4 (analog **43**) resulted in 10-fold potency increase for PDE10A with 15-fold concomitant potency decrease for PDE2 (**43** vs **30**). Furthermore, the similarly C4 methoxy substituted pyridyl analogs **44** and **45** were found to be the most potent and selective ligands of the pyridyl-triazine series of compounds, with IC_{50} values for PDE10A ~10 nM and >100–200 fold selectivity in the other PDE2-PDE6 isoforms. Compound **45** was further evaluated in PDE isoforms (PDE1, PDE7–PDE9, PDE11) and it was found to be weakly active (>500–1000 fold selective; data not shown).

Table 1
Pyridyl-triazine analogs

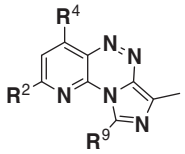

Compd	R^2	R^4	R^9	IC_{50}[a] (nM)					
				PDE10A	PDE2	PDE3	PDE4	PDE5	PDE6
30	OMe	H	4-Me-3-pyridyl	388	142	—	—	—	—
31	OMe	H	5-Me-3-pyridyl	51.5	14.4	—	—	—	—
32	OMe	H	5-OMe-3-pyridyl	91.3	14	—	—	—	—
33	OMe	H	2,4-Me, Me-thiazole	64.5	23	—	—	—	—
34	OMe	H	2-Me-Ph	47.6	15.8	>5000	>10,000	3410	1570
35	OMe	H	4-F, 2-Me-Ph	45.9	13.2	7260	>10,000	34100	1150
36	OMe	H	2-Cl-Ph	13.1	4.3	1240	>10,000	1680	435
37	OMe	H	2,4-Cl, Cl-Ph	15	15.1	>1000	>1000	>1000	>1000
38	OMe	H	2-Cl, 4-F-Ph	13.1	11.8	>1000	>1000	>1000	462
39	OMe	H	2,5-Cl, Cl-Ph	53.1	2.06	750	4410	1150	829
40	OMe	H	2-F, 5-OMe-Ph	9.83	2.99	1820	4820	702	734
41	OMe	H	2-F, 5-OEt-Ph	114	28.6	—	—	—	—
42	OMe	H	2-F, 5-O(CHMe$_2$)-Ph	2430	101.6	—	—	—	—
43	H	OMe	4-Me-3-pyridyl	42.4	1950	—	—	—	—
44	H	OMe	3-Me-4-pyridyl	10.1	2055	>10,000	3680	>10,000	>10,000
45	H	OMe	2-Me-3-pyridyl	12.4	974	>10,000	6960	>5000	>5000

[a] Means of IC_{50}; $n = 4$.

Table 2
Phenyl-triazine analogss

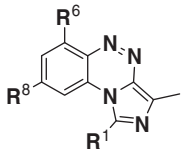

Compd	R^1	R^6	R^8	IC_{50}[a] (nM)					
				PDE10A	PDE2	PDE3	PDE4	PDE5	PDE6
46	2-Me-Ph	OMe	H	3.3	172	>10,000	176	3670	1980
47	2-Cl-Ph	OMe	H	2.41	103	>10,000	70.8	3060	1060
48	2-Cl-Ph	OMe	OMe	0.28	30.3	>5000	1910	436	73.15
49	2-Me-Ph	OMe	OMe	5.13	95.9	>10000	>10000	1110	349
50	2-CF_3-Ph	OMe	OMe	3.35	522	>1000	>1000	>1000	>1000
51	2-Me-3-pyridyl	OMe	OMe	1.48	196	>10,000	>10,000	1430	493
52	4-Me-3-pyridyl	OMe	OMe	4.16	775	>10,000	>10,000	5070	1822
53	3-Me-4-pyridyl	OMe	OMe	2.06	589	>10,000	>10,000	4950	1240
54	2-Me-Ph	OMe	morpholine	1.53	110	>10,000	2920	651	693
55	2-Cl-Ph	OMe	morpholine	0.85	50.4	>10,000	2680	603	276
56	3-Me-4-pyridyl	OMe	morpholine	3.99	4.37	>10,000	>10,000	5380	3120
57	2-OMe-Ph	OMe	F	6.53	894	>10,000	>10,000	>10,000	>10,000
58	3-OMe-Ph	OMe	F	9.11	1998	>1000	>1000	>1000	>1000
59	3-F, 2-Me-Ph	OMe	F	3.55	1150	>1000	>1000	>1000	>1000
60	4-Me-3-pyridyl	OMe	F	25.4	2375.5	>10,000	>10,000	>10,000	>10,000
61	3-Me-4-pyridyl	OMe	F	7.2	1220	>10,000	>10,000	>10,000	>10,000
62	2-Me-3-pyridyl	OMe	F	7.84	1270	>10,000	>10,000	>5000	2830
63	3,5-Me, Me-N-Me-pyrazole	OMe	F	13.1	1500	>10,000	>10,000	>10,000	>5000
64	3-Me-2-thienyl	OMe	F	1.65	269	>10,000	7720	3600	3270
65	2,4-Me, Me-thiazole	OMe	F	11.7	3420	>10,000	2460	4760	3880
66	3-Me-4-pyridyl	OMe	CF_3	1.48	346.5	>10,000	>10,000	2290	1790
67	4-Me-3-pyridyl	OMe	CF_3	5.11	864	>10,000	>10,000	>10,000	5250
68	3-F, 2-Me-Ph	OMe	CF_3	1.85	722	>5000	>5000	2130	1260
69	3-Me-4-pyridyl	OMe	OCF_2	7.0	944	>10,000	>10,000	4020	909
70	2-OMe-Ph	F	OMe	8.33	3390	>1000	>1000	>1000	>1000
71	3-Me-2-thienyl	F	OMe	9.43	35.9	2250	3670	2780	1230

[a] Means of IC_{50}; $n = 4$.

Next, we turned our attention to the evaluation of phenyl-fused triazines. In Table 2, we have aggregated selected analogs examining substitutions at positions 1, 6 and 8. Mostly, we have retained the methoxy group at position 6 of the phenyl-triazine scaffold, since it had played a key role to the potency and selectivity of the pyridyl-triazine PDE10A inhibitors, as described above. Tolyl

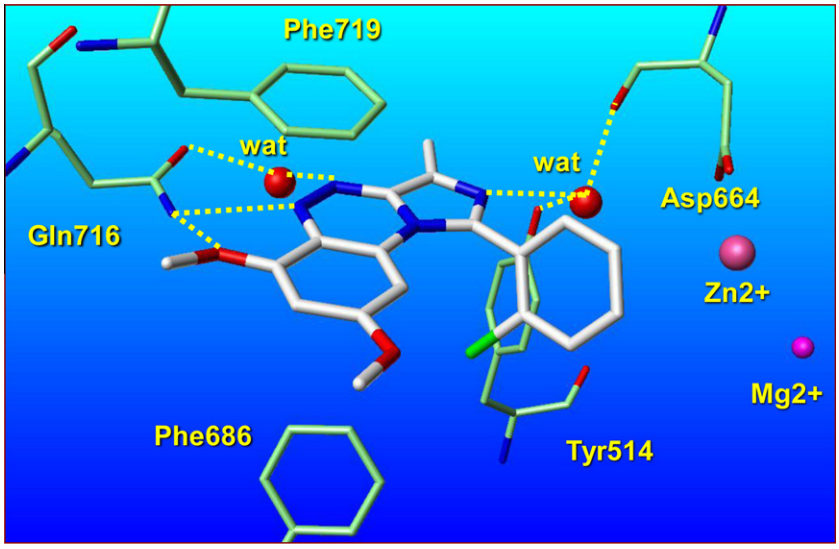

Figure 4a. Crystal structure (2.0 Å resolution; PDB ID code 4FCD) of PDE10A complexed with **48** highlighting the key hydrogen bond interactions between ligand and protein at the invariant Gln716 with both the triazine nitrogens and the 6-OMe group, and the water-mediated contacts with Asp664 and Thr623. The fused ring system of the ligand is sandwiched between residues Phe719, and Phe686, making p-stacking interactions with Phe719, p-edge stacking with Phe686. The C9 position 2-Cl-Ph rotates off the fused-tricyclic ring system about 90 degrees.

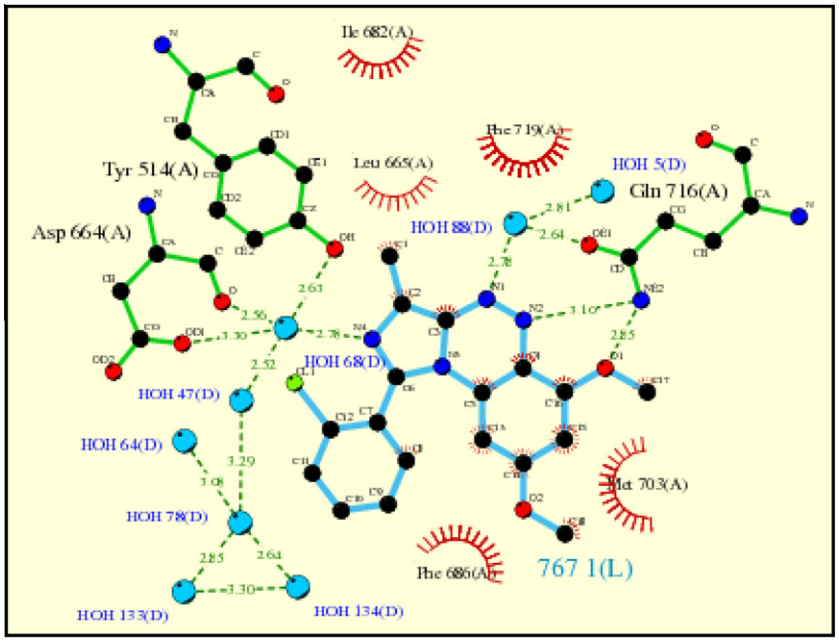

Figure 4b. Ligplot representation (2.0 Å resolution; PDB ID code 4FCD) of PDE10A complexed with **48** highlighting the hydrophobic and hydrogen bond interactions between the ligand and the amino acid residues involved in the PDE10A binding pocket.

analog **46** was a potent PDE10A inhibitor (IC_{50} = 3.3 nM) and about 60-fold selective against PDE2. Similar potency was also observed for the chloro-phenyl analog **47**. Nevertheless, both of these analogs inhibited PDE4 with IC_{50} values of 176 and 71 nM, respectively. Introduction of a methoxy group at position 8 (entry **48**) resulted in about 10-fold potency increase for PDE10A (**48** vs **47**), and a marked decrease (200×) of the PDE4 potency. Unexpectedly, compound **48** showed good potency for the PDE6 isoform (IC_{50} = 73 nM). In contrast, the analogous trifluoromethyl-phenyl analog **50** was about 10-fold weaker in PDE10A (**50** vs **48**), but inactive in PDE6, and the other tested PDEs. Dimethoxy analogs (entries **51**–**53**) with various pyridyl groups at position 1 have showed similar PDE10A potency to that of **50**, and better selectivity against PDE2. Amongst them, compound **53** was the most selective (~300×) against PDE2. Substitution at position 8 with a morpholine moiety (entries **54**–**56**) resulted in similar PDE10A potency to that of the C8 methoxy analogs but with significant decrease in selectivity against PDE2 (**56** vs **53**). The C8 substituted morpholine **56** was equipotent to both PDE10A and PDE2 isoforms, while the analogous C8 substituted methoxy analog **53** was about >280-fold selective against PDE2. Furthermore, introduction of a fluorine group at position 8 (entries **57**-**65**) exhibited similar PDE10A potency to that of the C8 methoxy analogs, while either retained or even enhanced selectivity against all tested PDE isoforms. Introduction of the more stable trifluoromethyl group (metabolically more stable than methoxy) at position 8 resulted in about

Table 3
Pharmacokinetic profile of selected compounds

Compd	**51**	**52**	**53**	**66**
Species	Rats	Rats	Rats	Rats
Dose; mg/kg	iv 2/po 10	iv 2/po 10	iv 2/po 10	iv 2/po 1
%*F*	100	100	100	53
$t_{1/2}$ (h)	2.0	0.8	0.9	4.5
CL (mL/min/kg)	4	14	13	5
Vss (L/kg)	0.4	0.5	0.4	1.3
AUC[a] $_{brain}$/AUC $_{plasma}$	6590/ 21,306	3001/ 8786	2781/ 18,681	622/ 1605

[a] AUC h*ng/mL

Table 4
Reversal of MK-801 induced hyperactivity and stereotyped sniffing

Compd	MED[a] hyperactivity (mg/kg po)	% Decrease in hyperactivity[b]	MED[a] sniffing (mg/kg po)	%Decrease in sniffing[b]	IC_{50} (nM)[c]
44	2.5	55.4	2.5	34.1	10.1
48	0.5	70.3	0.5	55.7	0.28
51	0.25	90.2	0.25	71.3	1.48
52	1	79.9	1	69.8	4.16
53	0.5	71.7	0.5	57.4	2.06
66	0.1	40.5	0.1	18.4	1.48
Clozapine	20	16.53	20	16.28	n.i.[d]

[a] Minimal effective dose that significantly reduced MK-801-induced hyperactivity or stereotyped sniffing, respectively, (p <0.05).
[b] p <0.001, n = 6.
[c] Inhibition of PDE10 activity from Tables 1 & 2.
[d] ni: no inhibition at PDE10.

threefold potency increase for PDE10A (**66** vs **61**, **67** vs **60**) with a modest twofold selectivity increase against PDE2. The C8 difluoromethoxy analog **69** was about 4-fold less potent (**69** vs **66**). Lastly, we have introduced a fluorine group at position 6 (entries **70**, **71**). The 2-methoxy phenyl analog **70** showed the highest selectivity against PDE2 (>400-fold), while the thienyl analog **71** was only threefold selective against PDE2 (**71** vs **64**). From the SAR findings described above, one can conclude that substitutions directed at the various sub-regions of the PDE10A ligand binding pocket influence collectively at various degree the selectivity of the compound against other known PDE isoforms, but most prominently against PDE2.

In support of our molecular modeling studies and design of PDE10A ligands, we have crystallized compound **48** with human PDE10A protein. Examination of the **48**:PDE10A crystal structure (Figs. 4a–b; PDB ID code 4FCD) revealed that the C9 2-chlorophenyl projects toward the opened space of the PDE10A binding pocket, in agreement with our molecular modeling calculations, and it is positioned practically in a vertical orientation relatively to the fused-ring system. Furthermore, the fused ring system of the ligand is sandwiched between residues Phe719 and Phe686, making π-stacking interactions with Phe719 and hydrophobic contacts with Phe686. Also, the ligand extends toward the invariant Gln716 residue and makes two direct hydrogen bond interactions between the C6 methoxy group and the position 5 nitrogen of the triazine nucleus, as well as a water mediated contact between the position 4 nitrogen of the triazine and Gln716. The ligand is further stabilized within the binding pocket with additional water-mediated hydrogen bonding interactions between the imidazole nitrogen and the residues Tyr514 and Asp664.

The majority of the analogs shown in Tables 1 and 2, have demonstrated good microsomal stability ($t_{1/2}$ > 30 min) in both human and rodent microsomes, have desired TPSA values (~50–65 Å^2), and good brain permeability (40%). Evaluation of selected PDE10 inhibitors in the MDR1-MDCK permeability assay revealed that the compounds showed high level of permeability [apical to basolateral (A–B) P_{app} and basolateral to apical (B–A) P_{app}] and lacked efflux properties (data not shown).

The evaluation of the pharmacokinetic properties of selected compounds in rats after oral administration is summarized in Table 3. All compounds showed low to moderate clearance, low volume of distribution, good oral bioavailability, moderate elimination terminal half-life ($t_{1/2}$) and good brain exposure.

Next, we evaluated this class of PDE10A inhibitors in models thought to be predictive of antipsychotic activity in humans.

Reversal of MK-801 induced hyperactivity in Rats: A representative subset of high affinity PDE10A inhibitors was selected for investigation of their antipsychotic-like potential in vivo. To enable the characterization of the antipsychotic activity we utilized a MK-801 induced hyperactivity reversal model where we have profiled the PDE10A mechanism previously.[23] MK-801 (0.1 mg/kg ip) significantly increased horizontal activity (t test: p <0.001) and induced stereotyped sniffing (t test: p <0.001) in female rats. These behaviors were significantly reversed by the positive control which in this case was the atypical antipsychotic clozapine. All evaluated PDE10A inhibitors also reversed hyperactivity and stereotyped sniffing in a dose dependent and significant manner. The minimal effective dose (MED) of the novel PDE10A inhibitors can be seen in Table 4. Compound **66** was the most active analog with a MED value of 0.1 mg/kg.

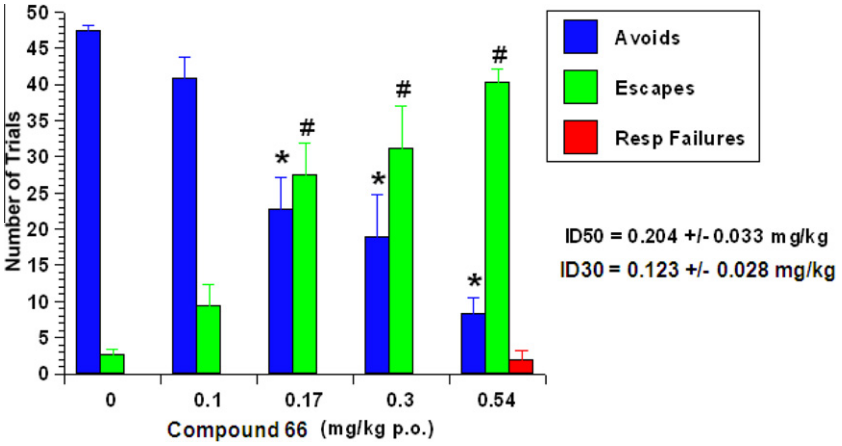

Figure 5. Compound **66** was evaluated in the conditioned avoidance response in male Sprague–Dawley rats using a 60-min pretreatment interval and an oral route of administration. Data are expressed as average (means S.E.M.; A) avoidance, escape, and response failures observed over 50 trials (n = 8 animals/group). *Statistical difference in avoidance and escape response from vehicle-treated controls (p = 0.05). Nonlinear regression analysis (B) calculated an ID_{50} equivalent to 0.204+/−0.033 mg/kg; p = 0.05.

Disruption of Conditioned Avoidance Responding (CAR) in Rats: Disruption of the 'avoidance' response in CAR is another preclinical model predictive of antipsychotic activity.[24,25] In the rat CAR model (Fig. 5), **66** decreased avoidance responding with a significant treatment effect at 0.17 mg/kg. Data are expressed as average (means S.E.M.) avoidance, escape, and response failures observed over 50 trials ($n = 8$ animals/group). Nonlinear regression analysis calculated an ID_{50} equivalent to 0.204+/−0.033 mg/kg; $p = 0.05$.

In this Letter, we have described the discovery of new pyridyl- and phenyl-triazine PDE10A inhibitors, further extending the SAR studies of previously disclosed[19] pyridyl- and phenyl- pyrazine PDE10A inhibitors. Applications of structure-based drug design techniques and molecular modeling have led to the identification of low-nanomolar PDE10A inhibitors with excellent selectivity against the other members of the PDE family. Particular attention was directed to the selectivity property of the PDE10A inhibitors against the PDE2 isoform, by methodically exploring the various sub-regions of the PDE10A ligand binding pocket to maximize ligand selectivity. A systematic assessment of the ADME and pharmacokinetic properties of the newly synthesized compounds has led to the design of drug-like candidates with good brain permeability and desirable drug kinetics ($t_{1/2}$, bioavailability, clearance). Compound **66** was highly potent for PDE10A ($IC_{50} = 1.4$ nM), demonstrated high selectivity (>250×) for the other PDEs (data not shown for PDE1, PDE7–PDE9, PDE11 isoforms in Table 2), and was efficacious in animal models of psychoses; reversal of MK-801 induced hyperactivity (MED = 0.1 mg/kg) and conditioned avoidance responding (CAR; ID_{50} = 0.204+/−0.033 mg/kg).

References and notes

1. Manallack, D. T.; Hughes, R. A.; Thompson, P. E. *J. Med. Chem.* **2005**, *48*, 3449.
2. Odingo, J. O. *Exp. Opin. Ther. Patents* **2005**, *15*, 773.
3. Rotella, D. *Nat. Rev. Drug Discov.* **2002**, *1*, 674.
4. Houslay, M. D.; Schafer, P.; Zhang, K. Y. *Drug Discov. Today* **2005**, *10*, 1503.
5. Bender, A. T.; Beavo, J. A. *Pharmacol. Rev.* **2006**, *58*, 488.
6. Loughney, K.; Snyder, P. B.; Uher, L.; Rosman, G. J.; Ferguson, K.; Florio, V. A. *Gene* **1999**, *234*, 109.
7. Fujishige, K.; Kotera, J.; Omori, K. *Eur. J. Biochem.* **1999**, *266*, 1118.
8. Fujishige, K.; Kotera, J.; Michibata, H.; Yuasa, K.; Takebayashi, S.; Okumura, K.; Omori, K. *J. Biol. Chem.* **1999**, *274*, 18438.
9. Soderling, S.; Bayuga, S. J.; Beavo, J. A. *Proc. Natl. Acad. Sci. U.S.A.* **1999**, *96*, 7071.
10. Soderling, S.; Beavo, J. A. *Curr. Opin. Cell Biol.* **1999**, *12*, 174.
11. Zhang, K.; Card, G.; Suzuki, Y.; Artis, R.; Fong, D.; Gillette, S.; Hsieh, D.; Neiman, J.; West, B.; Zhang, C.; Milburn, M.; Kim, S.-H.; Schlessinger, J.; Bollag, G. *Mol. Cell* **2004**, *15*, 279.
12. Seeger, T. F.; Bartlett, B.; Coskran, T. M.; Culp, J. S.; James, L. C.; Krull, D. L.; Lanfear, J.; Ryan, A. M.; Schmidt, C. J.; Strick, C. A.; Varghese, A. H.; Williams, R. D.; Wylie, P. G.; Menniti, F. S. *Brain Res.* **2003**, *985*, 113.
13. Coskran, T.; Morton, D.; Menniti, F.; Adamowicz, W.; Kleiman, R.; Ryan, A.; Strick, C.; Schmidt, C.; Stephenson, D. *J. Histochem. Cytochem.* **2006**, *54*, 1205.
14. Kaiya, H. *Prostaglandins Leukot. Essent. Fatty Acids* **1992**, *46*, 33.
15. Muly, E. C.; Smith, Y.; Allen, P.; Greengard, P. *Psychopharmacol. Bull* **2002**, *36*, 92.
16. Garver, D. L.; Carl Johnson, C.; Kanter, D. R. *Life Sci.* **1987**, *1982*, 31.
17. Giampa, C.; Laurenti, D.; Anzilotti, S.; Bernardi, G.; Menniti, F.; Fusco, F. *PLoS One* **2010**, *5*, e13417.
18. Hoefgen, N.; Stange, H.; Rudolf Schindler, R.; Lankau, H.-J.; Grunwald, C.; Langen, B.; Egerland, U.; Tremmel, P.; Pangalos, M. N.; Marquis, K. L.; Hage, T.; Harrison, B. L.; Malamas, M. S.; Brandon, N. J.; Kronbach, T. *J. Med. Chem.* **2010**, *53*, 4399.
19. Malamas, M. S.; Ni, Y.; Erdei, J.; Stange, H.; Schindler, R.; Hans-Joachim Lankau, H.-J.; Grunwald, C.; Fan, K.; Parris, K.; Langen, B.; Egerland, U.; Hage, T.; Marquis, K.; Harrison, B.; Robichaud, A.; Kronbach, T.; Pangalos, M.; Brandon, N.; Hofgen, N. *J. Med. Chem.* **2011**, *54*, 7621.
20. Verhoest, P.; Chapin, D.; Corman, M.; Fonseca, K.; Harms, J.; Hou, X.; Marr, E.; Menniti, F.; Nelson, F.; O'Connor, R.; Pandit, J.; Proulx-LaFrance, C.; Schmidt, A.; Schmidt, C.; Suiciak, J.; Liras, S. *J. Med. Chem.* **2009**, *52*, 5188.
21. Miyaura, N.; Suzuki, A. *Chem. Rev.* **1995**, *95*, 2457.
22. Stange, H.; Langen, B.; Egerland, U.; Hoefgen, N.; Priebs, M.; Malamas, M. S.; Edrei, J.; Ni, Y. U.S. Patents 0120762, 0120763, **2010.**
23. Grauer, S.; Pulito, V.; Navarra, R.; Kelly, M.; Kelley, C.; Graf, R.; Langen, B.; Logue, S.; Brennan, J.; Jiang, L.; Charych, E.; Egerland, U.; Liu, F.; Marquis, K.; Malamas, M. S.; Hage, T.; Comery, T.; Brandon, N. *J. Pharm. Exp. Ther.* **2009**, *331*, 574.
24. Li, M.; Fletcher, P. J.; Kapur, S. *Neuropsychopharmacology* **2007**, *32*, 263.
25. Smith, A.; Li, M.; Becker, S.; Kapur, S. *Neuropsychopharmacology* **2004**, *29*, 1040.